



# The First Results of Cloud Retrieval from Geostationary Environmental Monitoring Spectrometer

Bo-Ram Kim<sup>1,2</sup>, Gyuyeon Kim<sup>3</sup>, Minjeong Cho<sup>3</sup>, Yong-Sang Choi<sup>3,\*</sup> and Jhoon Kim<sup>4</sup>

<sup>1</sup>Satellite Application Division, National Satellite Operation and Application Center, Korea Aerospace Re-search Institute, Daejeon 34133, Republic of Korea

<sup>2</sup>Department of Atmospheric Science and Engineering, Ewha Womans University, Seoul 03760, Republic of Korea

<sup>3</sup>Department of Climate and Energy Systems Engineering, Ewha Womans University, Seoul 03760, Republic of Korea

<sup>4</sup>Department of Atmospheric Science, Yonsei University, Seoul 03722, Republic of Korea

Correspondence to: Yong-Sang Choi (ysc@ewha.ac.kr)

**Abstract.** This research introduces the cloud retrieval algorithm for Geostationary Environmental Monitoring Spectrometer (GEMS), the first geostationary orbit satellite, and shows the validation of its cloud products through comparison with other satellites: OMI, TROPOMI, AMI, and CALIOP. The purpose of GEMS cloud products is to correct the impact of clouds on atmospheric components retrieval, which use the O<sub>2</sub>-O<sub>2</sub> absorption band to retrieve the effective cloud fraction (ECF) and cloud centroid pressure (CCP). The GEMS cloud retrieval algorithm showed similar cloud retrieval performance to OMI. We analyzed the cloud retrieval characteristics for cases of air pollution, typhoons, and fog in the East Asia region to evaluate whether GEMS cloud products can represent various cloud features. The present cloud validation results would initiate to improve the GEMS cloud retrieval algorithm in the future.

## 1 Introduction

Since the start of Total Ozone Mapping Spectrometer (TOMS) in 1978 to monitor ozone layer changes, satellite remote sensing of atmospheric composition have been continuously operated. TOMS was followed by Ozone Monitoring Instrument (OMI), Global Ozone Monitoring Experiment (GOME), SCanning Imaging Absorption spectroMeter for Atmospheric CHartographY (SCIAMACHY), and the recent Tropo-spheric Monitoring Instrument (TROPOMI) (Hsu et al., 1997; Burrows et al., 1999; Bovensmann et al., 1999; Levelt et al., 2006; Veefkind et al., 2012). Recently, various satellites such as GHGSat, Greenhouse gases Observing SATellite (GOSAT), and Orbiting Carbon Observatory-2 (OCO-2) have been developed and operated to observe greenhouse gases to cope with climate change (Yoshida et al., 2011; Frankenberg et al., 2015; Jervis et al., 2021) Capabilities of satellite monitoring of atmospheric environment was extended to observe air pollutants including NO<sub>2</sub>, SO<sub>2</sub>, and aerosols, in addition to O<sub>3</sub> with spectrometers, using different spectral regions within the ultraviolet (UV)-visible (VIS) range of 240-790 nm with varying spectral resolutions of 0.2-0.4 nm depending on each satellite (Hsu et al., 1997; Burrows et al., 1999; Bovensmann et al., 1999; Levelt et al., 2006; Veefkind et al., 2012). Satellites are now employed to observe global warming by monitoring greenhouse gases(GHG) such as carbon dioxide and



methane using use spectrometers GHGs in the near-infrared and shortwave infrared regions (Yoshida et al., 2011; Frankenberg et al., 2015; Jervis et al., 2021).

In order to precisely retrieve concentration of atmospheric composition, it is necessary to accurately estimate the beam path length of the radiation that reaches the satellite. The beam path length represents the process of solar energy emitted from the sun being reflected on Earth and reaching the satellite, which is also determined by geometric factors such as solar zenith angle and satellite viewing angle. Clouds usually have a higher reflectance than most surfaces (excluding snow and ice) and exist above the surface. Therefore, cloud pixels have higher reflectance compared to clear-sky pixels, and the beam path length becomes shorter blocking the path of atmospheric composition below, which can result in errors in the observation of atmospheric environmental variables (Hong et al., 2017; Chimot et al., 2018). Therefore, it is necessary to evaluate and quantify the effects of clouds in order to obtain accurate atmospheric components' concentrations.

The cloud exhibits significant spatiotemporal variability, and its characteristics vary greatly depending on the spectral band. Therefore, to accurately estimate atmospheric components, it is necessary to derive real-time cloud information that reflects satellite instrument characteristics. Satellites for monitoring the atmospheric environment also operate their own algorithms to derive cloud information from each satellite. Thus, in previous studies, bands that mainly include phenomena by gases with relatively constant proportions in the dry atmosphere, such as Rotational Raman Scattering (RRS) (Joiner et al., 2006; Vasilkov et al., 2008), O<sub>2</sub>-O<sub>2</sub> absorption (Acarreta et al., 2004; Stammes et al., 2008; Veefkind et al., 2016; Vasilkov et al., 2018), and O<sub>2</sub>-A absorption bands (Wang et al., 2008; Wang et al., 2014; Loyola et al., 2018; Compennolle et al., 2021; Yang et al., 2021; Taylor et al., 2021), were mainly used for cloud retrieval. GOME, SCIAMACHY, and TROPOMI utilize the O<sub>2</sub>-A band to retrieve cloud information, while OMI without the O<sub>2</sub>-A band retrieves cloud information using two methods: the Raman scattering region and the O<sub>2</sub>-O<sub>2</sub> absorption band (Acarreta et al., 2004; Joiner et al., 2006; Stammes et al., 2008; Vasilkov et al., 2008; Wang et al., 2008; Vasilkov et al., 2018; Veefkind et al., 2016; Wang et al., 2018; Loyola et al., 2018; Compennolle et al., 2021). GOSAT and GHGSat utilize channels, including the O<sub>2</sub>-A band, for observing thin clouds and aerosols, and perform cloud screening and cloud cover estimation to consider the influence of clouds. The OCO-2 satellite also includes the O<sub>2</sub>-A band, which is used for cloud screening (Taylor et al., 2011; Yang et al., 2021).

The Geostationary Environmental Monitoring Spectrometer (GEMS) was launched in 2020 as the first geostationary environmental monitoring satellite in geostationary Earth orbit (GEO) (Kim et al., 2020). The GEMS is designed to monitor ozone, aerosols, nitrogen dioxide, sulfur dioxide, formaldehyde, and other atmospheric constituents in the UV-VIS range over the East Asia region. GEMS observes the wavelength range of 300-500 nm with a spectral resolution of 0.2 nm. As it operates in GEO, it is capable of observing the same field of view every hour. Previous satellites for atmospheric environmental monitoring were mainly operated in the sun-synchronous orbit (SSO) keeping the Sun-Earth-satellite angle constant, whereas GEMS operates in the GEO, making it essential to consider large variations in Solar Zenith Angle (SZA) and Viewing Zenith Angle (VZA). SZA varies greatly from dawn to noon and to sunset. While satellites in SSO perform observations close to noon for better illumination of Earth, a geostationary satellite operates throughout the day from dawn to sunset. Then, this leads to a decrease in the amount of radiation energy reaching the satellite and a longer beam path



65 length, which can result in errors in cloud retrieval. Therefore, the development and evaluation of algorithms that take these  
factors into account are crucial for accurate cloud retrieval (Kim et al., 2021a). Similarly, due to the wider observation range  
of the VZA compared to the low Earth orbit (LEO), errors may occur due to the increase in beam path length with the  
increase of the VZA. As this was the first time an environmental monitoring satellite was to be operated from a GEO, studies  
were conducted to consider the observation characteristics due to differences in orbit (Kwon et al., 2017; Kim et al., 2018;  
70 Bak et al., 2019; Go et al., 2020; Kim et al., 2021a).

In this study, we introduce a cloud retrieval algorithm for GEMS that takes into account the characteristics of observations  
from a GEO, and analyze the cloud properties retrieved from GEMS data. To ensure fast and stable operation, the GEMS  
cloud retrieval algorithm is designed based on a look-up table (LUT) that utilizes the O<sub>2</sub>-O<sub>2</sub> absorption band. The LUT was  
created assuming the range of values that can be observed under GEMS observation conditions for variables that affect O<sub>2</sub>-  
75 O<sub>2</sub> absorption, such as SZA, VZA, surface reflectance, and surface pressure. A detailed description of the cloud algorithm is  
provided in Section 2. To verify the performance of the algorithm, input data from OMI and TROPOMI were used, and for  
cloud product validation, Advanced Meteorological Imager (AMI) and Cloud-Aerosol Lidar with Orthogonal Polarization  
(CALIOP) cloud products were used for the validation. The introduction of the data is presented in Section 3, and the  
validation results are shown and discussed in Section 4. Section 5 provides a summary and overall evaluation of the GEMS  
80 cloud algorithm.

## 2 Geostationary Environmental Monitoring Spectrometer (GEMS) Cloud Algorithm

GEMS is operated onboard the Geostationary Korea Multipurpose Satellite-2B (GK-2B), a geostationary orbit program  
launched by South Korea in 2020, located at 128.2°E to provide continuous atmospheric observation of East Asia region. It  
is the first geostationary satellite designed to observe the 300-500 nm range with a resolution of 0.2 nm. As a UV-VIS  
85 observation satellite, GEMS observes the East Asian region (5°S - 45°N, 75°E - 145°E) at 1-hour intervals during daytime  
(00-09, 22-23 UTC) (Kim et al., 2020). The atmospheric components that GEMS aims to observe, such as ozone, nitrogen  
dioxide, sulfur dioxide, formaldehyde, glyoxal, and aerosols, can be affected by clouds, leading to reduced accuracy and  
even cases where some outputs are impossible to detect. In this section, the characteristics of clouds that cause errors in the  
estimation of atmospheric components' concentrations are defined (Section 2.1), and the retrieval algorithm is introduced  
90 (Section 2.2).

### 2.1 GEMS Cloud Products: Effective Cloud Fraction and Cloud Centroid Pressure

Visible and infrared region has been commonly used for cloud property retrieval mostly from weather satellites. It is very  
challenging to produce cloud properties in the UV-VIS region such as cloud top pressure and cloud phase. In the GEMS  
cloud algorithm, cloud products that can be corrected for the influence of clouds in a limited spectral range are defined and



95 produced. GEMS spectral range is limited to represent various cloud properties, therefore, it is assumed that the cloud is a simple reflective surface, rather than using a Mie scattering model that takes into account cloud phase, effective radius, etc. In the GEMS spectrum, clouds have higher reflectance compared to the surface except for snow and ice and are typically located at higher altitudes than air pollutants that GEMS is retrieving. Therefore, cloud products for atmospheric components estimation should be defined to correct for increased reflectance and beam path length. Thus, for the GEMS  
100 cloud retrieval algorithm, cloud products are defined using two parameters: Effective Cloud Fraction (ECF) and Cloud Centroid Pressure (CCP), which are also used in the O<sub>2</sub>-O<sub>2</sub> band algorithm (OMCLDO2) of OMI (Acarreta et al., 2004; Stammes et al., 2008; Veeffkind et al., 2016; Vasilkov et al., 2018).

The ECF is calculated (Eq. 1) by assuming a Lambertian Equivalent Reflectivity (LER) of 0.8 for clouds (Acarreta et al., 2004; Stammes et al., 2008), and comparing the observed reflectance ( $R_{obs}$ ) at a pixel with the simulated reflectance under  
105 clear-sky ( $R_{clr}$ ) and cloudy-sky ( $R_{cld}$ ) conditions.

$$ECF = \frac{R_{obs} - R_{clr}}{R_{cld} - R_{clr}} \quad (1)$$

A LER cloud model with a reflectivity of 0.8 is assumed to represent a sufficiently thick cloud with an optical thickness of approximately 30, and the effects of reflection within the cloud and multiple scattering that occurs beneath the cloud are ignored. The cloud model that defines the radiance of observed pixels by combining clear sky and cloudy sky pixels,  
110 assuming a reflectance of 0.8 for clouds and independent relationships between the two types of pixels (independent pixel approximation (Acarreta et al., 2004; Stammes et al., 2008; Veeffkind et al., 2016; Vasilkov et al., 2018)), is called the Mixed LER (MLER) model. The pressure at which reflection occurs due to the cloud is defined as the CCP. In addition, GEMS cloud algorithm defines cloud radiative fraction (CRF) for the wavelengths at which atmospheric components are retrieved, which provides the ratio of the radiance reflected by clouds to the observed radiance for the atmospheric components.  
115 Although GEMS produces three types of cloud products, this study only focuses on the comparison and verification of ECF and CCP excluding CRF, for the verification with other satellites.

## 2.2 GEMS Cloud Algorithm Description

In the GEMS cloud retrieval algorithm, the observed radiance (RAD) and irradiance (IRR) values, as well as the angle geometry information including SZA, VZA, and relative azimuth angle (RAA), and surface information such as surface  
120 pressure and surface reflectance are used as input values. During the operational testing of the GEMS cloud product algorithm, issues with the charge coupled device (CCD) in GEMS instrument were identified in some areas that were different from the original design, making observations above 485 nm impossible. Therefore, the algorithm was developed using the 460–485 nm range instead of the originally planned 460–490 nm range as input data for cloud retrieval algorithm.

Cloud detection is based on the reflection and scattering properties of clouds, making it possible to determine the presence of  
125 clouds throughout the GEMS spectrum. Cloud pressure is quantified by changes in the absorption or filling phenomena due to variations in the beam path length caused by clouds. However, it becomes difficult to quantify the impact of clouds when



the concentration of gases undergoes significant changes. Therefore, it is essential to select areas with minimal variation in trace gas concentrations.

130 The GEMS cloud retrieval algorithm assumes the MLER cloud model, which is the same as the cloud model assumption used in the OMI cloud product. Similarly to the O<sub>2</sub>-O<sub>2</sub> band-based cloud retrieval of OMI, the algorithm runs a radiative transfer model with inputs of angle geometry, surface information, ECF, and CCP. The algorithm uses a simulated result with a 0.6 nm interval in the 460-485 nm range to create a LUT. The detailed input values for the LUT are presented in Table 1. While OMI defines nodal points for angle geometry based on the angle spacing, GEMS defines nodal points for the LUT based on the cosine value of angle geometry to have a linear relationship with beam path length. This approach allows  
135 for the simulation of the LUT to be performed with a better linear interpolation scheme. For the radiative transfer simulation used to create the LUT, the Vector Linearized Discrete Ordinate Radiative Transfer (VLIDORT) NGST version (Spurr et al., 2006) was utilized and atmospheric profile is assumed by the profiles of the Deriving Information on Surface conditions from Column and Vertically Resolved Observations Relevant to Air Quality (DISCOVER-AQ) campaign (Flynn et al., 2014). The simulated radiance in the 460-485 nm range was converted to reflectance assuming the observed reflectance ( $R_\lambda$ )  
140 in Eq. 1 is the ratio between the simulated radiance and the irradiance.

The observed reflectance spectrum with a 0.6 nm interval in the 460-485 nm range are used as input data for the Differential Optical Absorption Spectroscopy (DOAS) method (Platt et al., 1979), as described by Equation (2), which quantifies O<sub>2</sub>-O<sub>2</sub> absorption.

$$\ln(-R_\lambda) = C_1 + C_2 \times \lambda + N_{s,o_2-o_2} \times \sigma_{o_2-o_2} + N_{s,o_3} \times \sigma_{o_3} \quad (2)$$

145 In equation (2),  $R_\lambda$  represents the 43 input observed reflectance spectra,  $\lambda$  represents the wavelength for the 43 reflectance spectra, and  $C_1$  and  $C_2$  are the offset and slope of the linear component, respectively.  $N_s$  represents the Slant Column Density (SCD), and  $\sigma$  refers to the absorption coefficient. In this study, only the effects of O<sub>2</sub>-O<sub>2</sub> and O<sub>3</sub> absorption were considered (Brion et al., 1998; Thalman et al., 2013). Therefore, only the column densities for O<sub>2</sub>-O<sub>2</sub> ( $N_{s, o_2-o_2}$ ) and O<sub>3</sub> ( $N_{s, o_3}$ ) absorption were calculated. The DOAS method separates the contribution of each gas's absorption coefficient as a weighting factor in  
150 regions where absorption occurs, providing a linear element and the SCD of each absorption coefficient from the input reflectance spectrum. The absorption coefficients of nitrogen dioxide also exist in the spectral range of the input reflectance, but the absorption by nitrogen dioxide is linear, so it was not considered as it has little effect on the quantification of O<sub>2</sub>-O<sub>2</sub> absorption. In contrast, absorption coefficient of ozone has a peak around 480 nm, and its absorption line is prominent in the case of upper-level clouds, affecting the quantification of O<sub>2</sub>-O<sub>2</sub> absorption, so it should be considered and removed.  
155 The LUT was constructed based on two intermediate products. The first intermediate product is the continuous reflectance (CR,  $R_c$ ) obtained by calculating the values of linear elements obtained through DOAS using equation (3).

$$R_c = C_1 + C_2 \times \lambda, \lambda = 477 \text{ nm} \quad (3)$$



The second intermediate product was based on the O<sub>2</sub>-O<sub>2</sub> SCD values obtained through DOAS. In the GEMS cloud retrieval algorithm, when the observed reflectance spectrum is provided, the intermediate products are first calculated via DOAS. 160 These intermediate products are then fed into a LUT along with angle geometry and surface information. Through a linear interpolation process, the final products, which are the ECF and CCP, are then produced.

Although GEMS cloud retrieval algorithm is generally similar to OMI cloud retrieval algorithm, there are significant differences in the process of generating LUT. As mentioned, since GEMS is located on a GEO, the VZA is constant for each location, but varies significantly across the observation area. On the other hand, the SZA varies significantly with time. 165 Therefore, in order to minimize the error of linear interpolation during the algorithm process, we defined the LUT using the cosine values of the zenith angle. In addition, different models were used to generate the LUT for the two algorithms. OMI used the DAK model (Acarreta et al., 2004; Stammes et al., 2008; Veeffkind et al., 2016; Vailkov et al., 2018), while GEMS used the VLIDORT NGST version. To account for the CCD issue that occurs in some observation areas of GEMS, the range of wavelengths for the input data in the DOAS analysis was adjusted to 460-485 nm.

### 170 3 Data and Method

In this section, four satellite data used for validating GEMS cloud retrieval algorithm are introduced in Section 3.1, collocation methods for comparison each satellite data in Section 3.2. To evaluate the performance of GEMS cloud retrieval algorithm, cloud products were produced using OMI radiance data, which has the most similar algorithm design. TROPOMI, a LEO environmental satellite that operates simultaneously with GEMS, was also used to analyze the characteristics of 175 clouds that appear during GEMS operation. In addition, AMI cloud data which is operated on the same orbit but with a different definition of clouds, and CALIOP data which observes the vertical distribution of clouds using an active sensor, were also used for validation.

#### 3.1 GEMS Cloud Algorithm Description

In this study, the GEMS cloud retrieval algorithm was designed and developed based on the OMI cloud retrieval algorithm, 180 which is a cloud product produced using O<sub>2</sub>-O<sub>2</sub> absorption. Therefore, OMI data was used as input data for algorithm validation testing. OMI is a UV-VIS observation satellite launched in 2004 and onboard Aura in the A-train, observing the 270-500 nm range at intervals of 0.6 (Levelt et al., 2006). In addition to ozone, it also produces sulfur dioxide, nitrogen dioxide, and two types of cloud products: OMCLDRRS, which uses RRS near 388 nm (Joiner et al., 2006; Vasilkov et al., 2008), and OMCLDO2, which uses the O<sub>2</sub>-O<sub>2</sub> absorption in the 460-490 nm range (Acarreta et al., 2004; Stammes et al., 185 2008; Veeffkind et al., 2016; Vailkov et al., 2018). The cloud pressure is determined based on the scattering/absorption characteristics that vary with the presence of clouds in OMCLDRRS and OMCLDO2. RRS determines cloud pressure based on the phenomenon where absorption lines formed by radiation emitted from the sun are filled by non-elastic scattering as they pass through the Earth's atmosphere. In contrast, OMCLDO2 determines cloud pressure by utilizing the absorption



190 characteristics generated by collisions of O<sub>2</sub> molecules with almost constant mixing ratio in dry air. It is known that the RRS  
method produces pressure closer to cloud top pressure than the O<sub>2</sub>-O<sub>2</sub> method (Sneep et al., 2008; Joiner et al., 2012).  
Additionally, each algorithm is advantageous for detecting high and low clouds, respectively, based on the characteristics of  
scattering/absorption used in each algorithm.

195 OMI observation data can be used as input data to evaluate the characteristics of the GEMS cloud algorithm by excluding  
errors caused by satellite orbit, viewing geometry, and resolution (Park et al., 2020; Park et al., 2021). We used OMI RAD  
and IRR observed on randomly selected days each month in 2007 as input data for the algorithm. OMI provides surface  
reflectivity values for 36 channels, which are essential input data for cloud retrieval, and the GEMS cloud algorithm used  
surface reflectivity values at 463 nm adjacent to O<sub>2</sub>-O<sub>2</sub> absorption band, the same as the OMI algorithm (Kleipool et al.,  
2008).

200 TROPOMI uses the O<sub>2</sub>-A absorption around 760 nm to produce cloud products for cloud correction. The cloud products  
include Cloud Fraction (CF), Cloud Top/Bottom Pressure (CTP, CBP), cloud optical thickness, and various other cloud  
information. TROPOMI, a successor environmental observation satellite of OMI, is equipped with four spectrometers that  
observe from UV to shortwave infrared, including 760 nm. Therefore, it can provide higher accuracy in surface and cloud  
product compared to GEMS. Launched in 2017, TROPOMI operates on a SSO like OMI and has a spatial resolution of 5.5 ×  
7 km<sup>2</sup> similar to GEMS, making it useful for testing and validation of initial GEMS results. This study verifies the retrieved  
205 cloud products using TROPOMI data.

TROPOMI observed the UV-VIS spectrum on the SSO and was mainly used as experimental data and reference for GEMS  
algorithms (Wang et al., 2020; Kang et al., 2020; Choi et al., 2020; Lee et al., 2020; Baek et al., 2022). TROPOMI was also  
used as input data for cloud products to evaluate the performance of GEMS cloud algorithms. In this study, TROPOMI  
provides RAD, IRR, surface reflectance, pressure, and angle geometry were used to evaluate the performance of cloud  
210 algorithms. In addition, to analyze the characteristics of clouds observed from different orbits, GEO and SSO, verification  
was performed using data observed on the same day and at the same time (within 15 minutes) as GEMS observations.

The CALIOP satellite, which is often used for qualitative cloud verification, produces a vertical feature mask of clouds  
through active sensors. CALIOP is a lidar satellite instrument that was launched in 2006 as part of The Cloud-Aerosol Lidar  
and Infrared Pathfinder Satellite Observation (CALIPSO) program, which aims to observe clouds and aerosols that have a  
215 significant impact on Earth's weather and climate (Winker et al., 2009). It receives backscattered energy from two bands at  
532 nm and 1064 nm using three receivers, providing information on the vertical distribution of clouds and aerosols. In this  
study, we qualitatively compared the cloud products produced by different bands using the L2-VFM data, which is a cloud-  
aerosol profile.

220 The comparison of cloud detection characteristics between meteorological and environmental satellites with different  
spectral range, which operate in GEO, can provide insights into the differences in cloud properties depending on the spectral



bands. AMI, which produces the most diverse cloud products such as cloud pressure, cloud phase, cloud optical thickness, and effective particle radius, is a meteorological sensor onboard GK-2A, which observes 16 bands in the 0.5 to 13.3  $\mu\text{m}$  range. Since the main purpose of weather observation is to observe various weather phenomena, various cloud properties are defined and produced, where cloud detection is performed by simultaneously utilizing the visible and infrared regions. CTP  
225 is mainly based on the infrared channels (Kim et al., 2019), and cloud pressure in this case has a less sensitive characteristic to low clouds due to reduced thermal contrast (Miller et al., 2012).

### 3.2 Validation Method

Validation was conducted in two ways: one to evaluate the performance of the algorithm itself, excluding the differences in observation sensors, and the other to understand the characteristics of the cloud products produced from actual observations  
230 in GEMS. For evaluating algorithm performance, radiance data and cloud products from OMI and TROPOMI, which observe spectrum in the UV-Vis range, were used. For comparing the characteristics of GEMS cloud products, TROPOMI, CALIOP, and AMI, which provide cloud products and data observed at the similar time to GEMS, were used as validation data (Sneep et al., 2008; Kim et al., 2019).

For the evaluation of the GEMS cloud algorithm performance using OMI and TROPOMI spectrum, a collocation process is  
235 not required. In addition, for OMI, which is based on the same cloud model as GEMS, the cloud definitions derived are identical in terms of ECF and CCP, making it possible to compare without any preprocessing. However, for TROPOMI, although clouds are assumed to be LER like GEMS, the cloud albedo is assumed to be 1.0, not 0.8, so the TROPOM CF needs to be converted to cloud effective amount prior to the comparison using the equation (4) and ECF of GEMS (Loyola et al., 2018).

$$240 \quad \text{ECF} = \text{CF} \times \frac{1.0}{0.8} \quad (4)$$

Moreover, the cloud pressure from TROPOMI is provided as separate cloud top and cloud base pressures, thus, to compare with GEMS, which only provides cloud center pressure, the median value was calculated for validation.

To verify various cloud characteristics, cases of high aerosol concentration, typhoons, and fog were selected when the GEMS, AMI, TROPOMI, and CALIOP satellites passed over the Korean Peninsula. To validate satellite data from different  
245 orbits, a spatiotemporal collocation was necessary. TROPOMI and CALIOP passed the Korean Peninsula around local time 13:30. Since GEMS observes the Korean Peninsula at  $\sim 45$  minute past every hour during daytime, data observed at 13:45 was selected as the validation data. AMI observed the Korean Peninsula every 10 minutes, using data observed at 13:40 for validation.

AMI provides cloud detection results with a spatial resolution of  $2 \text{ km} \times 2 \text{ km}$ . To compare with ECF, collocation was  
250 performed to select pixels that are included in the GEMS observation pixel, and the CF was calculated by counting the number of cloud pixels for comparison. CTP is the mean CTP value of cloud pixels. However, it is difficult to perform



quantitative verification of CCP from GEMS and CTP from CALIOP or AMI, as they represent cloud pressure with different definition. VFM can evaluate the validity of cloud detection and estimation as it provides cloud vertical distribution. CCP is converted to Cloud Centroid Height (CCH) using Equation (5) for qualitative verification of cloud pressure.

$$255 \quad CCH = -h_{scale} \ln\left(\frac{CCP}{p_s}\right) + h_s \quad (5)$$

with  $p_s$  the surface pressure and  $h_s$  the surface altitude of GEMS pixel. The value of 7710 m was obtained by fitting to the atmosphere profile from DISCOVER-AQ campaign (Flynn et al., 2014), which is used as a reference in the GEMS cloud retrieval algorithm. For spatial collocation, the nearest neighbor method was based on the CALIOP observation pixels which has the narrowest swath. The same method was applied for GEMS and TROPOMI collocation, with comparison performed  
260 between the nearest pixels.

## 4 GEMS Cloud Algorithm Results Using OMI and TROPOMI Radiances

### 4.1 Comparison with OMI Clouds

To evaluate the performance of the GEMS cloud algorithm, which was designed based on the same theoretical background as the OMI's OMCLDO2 algorithm. Figure 1 examines the characteristics of cloud products according to the season using  
265 observational data for random days of each month in 2007. To represent the seasons, the analysis was performed using observational data for January, February, and December (DJF) for winter, March, April, and May (MAM) for spring, June, July, and August (JJA) for summer, and September, October, and November (SON) for autumn. We draw density scatter plots for comparison of the two products, and analyzed the correlation between them through linear regression. The x-axis represents the cloud products calculated and provided by OMI, while the y-axis represents the cloud products calculated by  
270 the GEMS cloud algorithm using OMI level1B data as input. The top panel of Figure 1 shows a density scatter plot of ECF, while the bottom panel shows a density scatter plot of CCP, and the solid line represents the 1:1 line.

The ECF showed similar values between GEMS and OMI across the entire study area, regardless of cloud amount. The correlation coefficient was high, ranging from about 0.92 to 0.95, and the regression line slope was also close to 1, ranging from 0.9 to 0.94, indicating a strong agreement between GEMS and OMI. The Root Mean Square Error (RMSE) and Mean  
275 Bias Error (MBE) were 0.12 and -0.01, respectively, and large errors were mainly observed in areas with small ECF values. Overall, the correlation coefficient and slope for ECF between the two satellites did not show significant seasonal differences, indicating that the algorithm design did not result in significant seasonal bias in the performance of the cloud retrieval algorithm.

Similar to ECF, GEMS also produced CCP values similar to OMI for the entire domain. However, for areas with ECF less  
280 than 0.2, the accuracy of CCP retrieval using O<sub>2</sub>-O<sub>2</sub> absorption is significantly lower (Vasilkov et al., 2008; Sneep et al., 2008; Loyola et al., 2018; Compornolle et al., 2021). Therefore, validation is for only pixels with ECF greater than 0.2. Both



OMI and GEMS had approximately 50% of the pixels with ECF greater than 0.2. The correlation coefficient was around 0.95 for all seasons, and the regression line slope was above 0.9, indicating that GEMS produced CCP similar to OMI regardless of the season.

285 Figure 2 shows the retrieved ECF and CCP over the GEMS FOV using OMI data from March 25th, 2007. Three swaths which covered through from 03 to 06 UTC of OMI data covering the GEMS FOV were selected for analysis. (a) and (b) show the ECF retrieved by OMI and GEMS, respectively. The (c) shows the difference between the ECF retrieved by OMI and GEMS. (d) and (e) show the CCP retrieved by OMI and GEMS, respectively, while (f) shows the difference between the CCP retrieved by the two algorithms. The retrieved ECF showed similar errors in each swath, with the errors being most  
290 prominent in areas with low ECF and the edge in RAA. These errors were found to be strongly correlated ( $\sim 0.8$ ) with RAA. Since GEMS is operated from a geostationary orbit, consideration of RAA was minimized in the algorithm, because the discontinuous azimuth angle observed by polar-orbiting satellites such as OMI is reduced in geostationary orbit. This could be a major source of the differences between the two algorithms.

#### 4.2 Comparison with TROPOMI Clouds

295 We evaluated the performance of the GEMS cloud retrieval algorithm using TROPOMI data, which can be observed simultaneously with GEMS, taking into account the differences in the orbit and spectral range of observation. Similar to the experiments in Section 4.1, we conducted quantitative validation (Figure 3) and qualitative validation (Figure 4) for randomly selected days in March, June, September, and December 2021. Since TROPOMI cloud retrieval products are defined differently from GEMS, we converted the CF provided by TROPOMI to ECF using Equation (4) to represent the  
300 cloud amount and used the mean values of CTP and CBP (mean Cloud Pressure, mCP) for validation with CCP. We performed cloud retrieval and analysis for three swaths (observation time 03-06 UTC) covering East Asia, which is the FOV of GEMS. Figure 3 shows the results for March, June, September, and December from left to right, with the top panels showing the results for ECF and the bottom panels showing the density scatter plot for CCP. The x-axis in the top panel represents the converted CF values from TROPOMI to ECF, and the y-axis represents the ECF values obtained from GEMS  
305 using TROPOMI L1B radiance as input. The x-axis in the bottom panel for CCP represents the median values of CTP and CBP obtained from TROPOMI, and the y-axis represents GEMS CCP using TROPOMI as input. There was no noticeable difference in the algorithm's performance for each season. However, for the ECF, since we corrected and compared the products with different definitions, it was found that the linear relationship was not clear and the correlation coefficients were relatively low compared to Figure 1.

310 Figure 4 shows the ECF (top) and CCP (bottom) obtained from TROPOMI (left) and GEMS (right) on September 16, 2021. The difference in ECF is pronounced in the Tibetan Plateau region, and overall, there is a noticeable difference in ECF between ocean and land areas. This is due to the fact that TROPOMI does not provide surface reflectance at 463 nm and instead uses surface reflectance at 420 nm as input data. As for CCP, it is difficult to compare with TROPOMI mCP as the definitions differ significantly, but overall, it was found that GEMS CCP is lower in altitude than TROPOMI mCP.



## 315 5 GEMS Cloud Algorithm Results Using GEMS Radiances

Using observation data from GEMS, the accuracy and usability of the cloud products retrieved by the GEMS cloud algorithm were evaluated by comparing them with cloud products produced by other sensors and orbits, such as TROPOMI, AMI, and CALIOP, based on data collected after the in-orbit test completed in 2021. In particular, three cases of high concentrations of fine dust, typhoons, and sea fog were selected to reflect the atmospheric environment and cloud characteristics in East Asia. The results of the comparison verification were described in this section.

### 5.1 Air Pollution Case

The main purpose of GEMS is to monitor air pollutant in the East Asian region, therefore we selected a high air pollutant case. To analyze the characteristics of clouds that appear during high concentrations of fine dust, which occurred in May 2021, Figures 5 and 6 were used to show cloud detection and cloud pressure, respectively. The data analyzed was taken around 0430 UTC, when the A-train was passing, and the 0445 UTC data was analyzed based on GEMS FOV. Figure 5(a) shows the ECF result of GEMS, Figure 5(b) shows the ECF result of TROPOMI, Figure 5(c) shows the CF image of AMI, and Figure 5(d) shows the aerosol optical depth (AOD) image derived from AMI.

Comparing GEMS and AMI clouds, it is easy to grasp that AMI detects many more areas as clouds compared to GEMS. AMI is operated to observe meteorological phenomena, particularly those closely related to meteorological phenomena, so it has the characteristic of detecting clouds very sensitively. When comparing TROPOMI and GEMS cloud fraction in (c), they are almost similar in shape, confirming that they detect clouds in a similar sensitivity. The GEMS cloud retrieval algorithm uses surface reflectance climatology from OMI as input data, the surface properties in the ECF is revealed as it is since the surface reflectance data is not updated. In (d), which represents AMI AOD, the high-concentration fine dust belt in the southern region of the Korean Peninsula can be easily observed. GEMS and TROPOMI both detected a very thin cloud (ECF < 0.2) in this region. So far, the cloud production algorithms of GEMS and TROPOMI do not provide additional information on aerosols, and it seems difficult to classify aerosols from cloud and it is challenges in GEMS cloud production algorithm.

Figure 6 shows the CCP validation result observed on the same day as Figure 5. The (a) displays the GEMS CCP, while the (b) shows the TROPOMI mCP. The (c) shows the CTP provided by AMI, and the (d) is an image overlaying the cloud products of three satellites on the CALIOP VFM. In (d), black dots represent GEMS CCP, blue dots represent AMI CTP, gray shading represents the range between TROPOMI CTP and CBP, pink shading represents the region where clouds were detected by CALIOP VFM, and orange shading represents the region where aerosols were detected. To compare with CALIOP VFM, the CCP analysis figures, such as Figure 6, were showed in height unit using Equation (4) with the unit converted to height.

The cloud height (CH) results obtained in Figure 6. (a) - (c) exhibit distinctive characteristics for each satellite that make it difficult to find commonalities. GEMS produced values that are similar to surface height for clear pixels, while for areas with aerosols, it retrieved CH values within the range of aerosol existence. The cloud retrieval algorithm used by GEMS



cannot distinguish between clouds and aerosols, and the scattering effect at the wavelengths used for cloud retrieval causes the cloud altitude to be calculated as if there were clouds when there are aerosols present, due to the reflection effect caused by aerosols. Comparing TROPOMI CTH, CBP with GEMS's CCH revealed that, in general, GEMS tends to estimate lower  
350 cloud heights than TROPOMI cloud pressure.

## 5.2 Typhoon Case

Typhoons are a meteorological phenomenon that brings a wide variety of clouds, making them a useful case for cloud verification. Typhoon Chantu, which occurred in September 2021, was a large typhoon, where it is located to the southwest of the Korean Peninsula, as can be easily seen in all (a) - (c) images in Figure 7. Figure 7 contains the results of each  
355 satellite's cloud detection, as in Figure 5, but excludes verification of AOD because we focused on clouds. As a well-developed tropical low-pressure system, a typhoon accompanies various types of clouds, ranging from thick clouds to cirrus clouds, providing various aspect on how GEMS retrieves different types of clouds. It was observed in (a) that the ECF is significantly high around the eye of the typhoon. TROPOMI and AMI also showed high agreement in cloud detection for thick clouds.

360 Typhoons bringing various type of clouds are useful for understanding the general characteristics of cloud distribution. However, in cases where the clouds are thick enough, the active sensor CALIOP has limited penetration and may not provide sufficient information below the clouds. Comparing cloud height from (a) to (c), GEMS cloud height is lower than other satellites in general, we analyze the vertical structure of the clouds for details through Figure 8. (d). In (d), the VFM of typhoon clouds being reported only in the upper atmosphere can also be attributed to the thick clouds. AMI, which produces  
365 cloud top height in (d), reports clouds at high altitudes similar to CALIOP VFM, except for the typhoon eye. CH produced by GEMS and TROPOMI also accurately detect the typhoon eye, and as shown in Figure 6, GEMS tends to underestimate cloud height compared to TROPOMI. In addition, while AMI produced CTH in the upper atmosphere for areas estimated to be multi-layered above 40 degrees latitude, GEMS CCP tended to produce CH in the lower layer. These characteristics can be useful for understanding the properties of multi-layered clouds in the further study.

## 370 5.3 Sea Fog Case

Sea fog is a common phenomenon in the western coast of Korea and can be included in the transport path of air pollutants. Therefore, false detection of sea fog can lead to significant errors in the observation of atmospheric pollutants using GEMS. In this section, we choose a sea fog case to analyze the performance of GEMS cloud products to determine which cloud is  
375 retrieved in the sea fog case. In Figure 9, sea fog is difficult to distinguish from low-level clouds over the ocean by naked eyes, but can be identified as fog by observing its movement over time from geostationary satellites. Unlike clouds, sea fog tends to linger near the coast and does not have much flow. It was found that all three cloud fraction, GEMS, TROPOMI, and AMI, detected the presence of sea fog as clouds.



As sea fog induces high reflectance, accurate retrieval of CCP is essential for correcting atmospheric pollutant observations. In the case of GEMS, sea level pressure can be obtained for areas suspected of sea fog, it is useful for correcting the influence of sea fog on atmospheric components retrievals. TROPOMI, which uses the NIR region for cloud retrieval, also retrieves CP in sea fog areas close to the surface altitude, and AMI shows a tendency to retrieve CH like low-level clouds. If the CH in GEMS is overestimated, as in the case of AMI, it may cause an overestimation of atmospheric components.

## 6 Conclusions and Discussions

In this study, we introduce the GEMS cloud algorithm and compare and validate its results. The GEMS cloud algorithm is based on the cloud retrieval algorithm of the preceding polar-orbiting satellite, OMI, and therefore produces very similar values to OMI's cloud products with a correlation coefficient of over 0.94 for all seasons. Although it was difficult to make quantitative comparisons due to different cloud definitions, we also performed validation using data from TROPOMI, a UV-VIS environmental satellite currently in operation. The effective cloud fraction was generally similar, and the cloud centroid pressure was found to be located between TROPOMI cloud top pressure and cloud bottom pressure, showing that it is appropriate for use in trace gas correction.

Since GEMS operates in geostationary orbit, unlike previous environmental satellites, it is important to detect diurnal cloud characteristics that appear over the East Asian region. Therefore, in this study, examples of air pollutants, typhoons, and sea fog cases easily observed in the East Asian region were selected to compare and verify the cloud results of GEMS with those of other satellites. Cloud heights produced by GEMS, TROPOMI, and AMI were compared based on CALIOP vertical feature mask, which can observe the vertical distribution of clouds. CALIOP was found to be insufficient in detecting low clouds when there are thick clouds, and GEMS was found to detect cloud heights the lowest among the four satellites, representing the reflecting height. The cloud top height produced by TROPOMI was located at a lower altitude than AMI cloud top height, and GEMS CH is usually located between CBH and CTH. AMI generally produced CTH that closely matched top of CALIOP VFM, but tended to overestimate CH in the sea fog case. Through comparison of GEMS ECF and CCP in cases, it was confirmed that the cloud characteristics were well reflected in the retrieval results, and it is expected to be useful for correcting the beam path length of observed radiation.

The current version of the GEMS cloud algorithm generates results consistent with the cloud output produced by other satellites and seems to accurately reflect cloud characteristics in East Asia. However, there are major two issues that have been pointed out, (1) the reflectivity and pressure characteristics of inland regions, including the Tibetan Plateau, being directly reflected in the derived ECF, and (2) most regions showing the ECF greater than zero. This is due to the current algorithm using OMI climatology as input values for surface reflectance. The surface reflectance from OMI is difficult to represent the current surface due to the influence of changes in background aerosols in the atmosphere, among other factors



(M. Kim et al., 2021). In the next version of the algorithm update, it is planned to replace the input value with surface  
410 reflectance observed by GEMS, which is expected to solve both problems.

## Funding

This subject is supported by Korea Ministry of Environment (MOE) as Public Technology Program based on Environmental Policy (2017000160003).

## References

- 415 Acarreta, J., De Haan, J., and Stammes, P.: Cloud pressure retrieval using the O<sub>2</sub>-O<sub>2</sub> absorption band at 477 nm, *Journal of Geophysical Research: Atmospheres*, 109, 2004.
- Baek, K., Kim, J. H., Bak, J., Haffner, D. P., Kang, M., and Hong, H.: Evaluation of total ozone measurements from Geostationary Environmental Monitoring Satellite (GEMS), *EGUsphere*, 1-23, 2022.
- Bak, J., Baek, K.-H., Kim, J.-H., Liu, X., Kim, J., and Chance, K.: Cross-evaluation of GEMS tropospheric ozone retrieval  
420 performance using OMI data and the use of an ozonesonde dataset over East Asia for validation, *Atmospheric Measurement Techniques*, 12, 5201-5215, 2019.
- Bovensmann, H., Burrows, J., Buchwitz, M., Frerick, J., Noel, S., Rozanov, V., Chance, K., and Goede, A.: SCIAMACHY: Mission objectives and measurement modes, *Journal of the atmospheric sciences*, 56, 127-150, 1999.
- Brion, J., Chakir, A., Charbonnier, J., Daumont, D., Parisse, C., and Malicet, J.: Absorption spectra measurements for the  
425 ozone molecule in the 350–830 nm region, *Journal of atmospheric chemistry*, 30, 291-299, 1998.
- Burrows, J. P., Weber, M., Buchwitz, M., Rozanov, V., Ladstätter-Weissenmayer, A., Richter, A., DeBeek, R., Hoogen, R., Bramstedt, K., and Eichmann, K.-U.: The global ozone monitoring experiment (GOME): Mission concept and first scientific results, *Journal of the Atmospheric Sciences*, 56, 151-175, 1999.
- Chimot, J., Veeffkind, J. P., Vlemmix, T., and Levelt, P. F.: Spatial distribution analysis of the OMI aerosol layer height: a  
430 pixel-by-pixel comparison to CALIOP observations, *Atmospheric Measurement Techniques*, 11, 2257-2277, 2018.
- Choi, W., Lee, H., Kim, J., and Park, J.: First TROPOMI Retrieval of Aerosol Effective Height Using O<sub>4</sub> Absorption Band at 477 nm and Aerosol Classification, *IEEE Transactions on Geoscience and Remote Sensing*, 59, 9873-9886, 2020.
- Compernelle, S., Argyrouli, A., Lutz, R., Sneep, M., Lambert, J.-C., Fjæraa, A. M., Hubert, D., Keppens, A., Loyola, D., and O'Connor, E.: Validation of the Sentinel-5 Precursor TROPOMI Cloud Data with Cloudnet, Aura OMI O<sub>2</sub>-O<sub>2</sub>, MODIS, and  
435 Suomi-NPP VIIRS, *Atmospheric Measurement Techniques*, 14, 2451-2476, 2021.
- Flynn, C. M., Pickering, K. E., Crawford, J. H., Lamsal, L., Krotkov, N., Herman, J., Weinheimer, A., Chen, G., Liu, X., and Szykman, J.: Relationship between column-density and surface mixing ratio: Statistical analysis of O<sub>3</sub> and NO<sub>2</sub> data from the July 2011 Maryland DISCOVER-AQ mission, *Atmospheric Environment*, 92, 429-441, 2014.



- Frankenberg, C., Pollock, R., Lee, R., Rosenberg, R., Blavier, J.-F., Crisp, D., O'Dell, C., Osterman, G., Roehl, C., and  
440 Wennberg, P.: The Orbiting Carbon Observatory (OCO-2): spectrometer performance evaluation using pre-launch direct sun  
measurements, *Atmospheric Measurement Techniques*, 8, 301-313, 2015.
- Go, S., Kim, J., Park, S. S., Kim, M., Lim, H., Kim, J.-Y., Lee, D.-W., and Im, J.: Synergistic use of hyperspectral uv-visible  
omi and broadband meteorological imager modis data for a merged aerosol product, *Remote Sensing*, 12, 3987, 2020.
- Hong, H., Lee, H., Kim, J., Jeong, U., Ryu, J., and Lee, D. S.: Investigation of simultaneous effects of aerosol properties and  
445 aerosol peak height on the air mass factors for space-borne NO<sub>2</sub> retrievals, *Remote Sensing*, 9, 208, 2017.
- Hsu, N. C., McPeters, R. D., Seftor, C. J., and Thompson, A. M.: Effect of an improved cloud climatology on the total ozone  
mapping spectrometer total ozone retrieval, *Journal of Geophysical Research: Atmospheres*, 102, 4247-4255, 1997.
- Jervis, D., McKeever, J., Durak, B. O., Sloan, J. J., Gains, D., Varon, D. J., Ramier, A., Strupler, M., and Tarrant, E.: The  
GHGSat-D imaging spectrometer, *Atmospheric Measurement Techniques*, 14, 2127-2140, 2021.
- 450 Joiner, J. and Vasilkov, A. P.: First results from the OMI rotational Raman scattering cloud pressure algorithm, *IEEE  
transactions on geoscience and remote sensing*, 44, 1272-1282, 2006.
- Joiner, J., Vasilkov, A., Gupta, P., Bhartia, P., Veefkind, P., Sneep, M., de Haan, J., Polonsky, I., and Spurr, R.: Fast  
simulators for satellite cloud optical centroid pressure retrievals; evaluation of OMI cloud retrievals, *Atmospheric  
Measurement Techniques*, 5, 529-545, 2012.
- 455 Kang, M., Ahn, M.-H., Liu, X., Jeong, U., and Kim, J.: Spectral calibration algorithm for the geostationary environment  
monitoring spectrometer (GEMS), *Remote Sensing*, 12, 2846, 2020.
- Kim, H.-S., Baum, B. A., and Choi, Y.-S.: Use of spectral cloud emissivities and their related uncertainties to infer ice cloud  
boundaries: methodology and assessment using CALIPSO cloud products, *Atmospheric Measurement Techniques*, 12, 5039-  
5054, 2019.
- 460 Kim, G., Choi, Y.-S., Park, S. S., and Kim, J.: Effect of solar zenith angle on satellite cloud retrievals based on O<sub>2</sub>-O<sub>2</sub>  
absorption band, *International Journal of Remote Sensing*, 42, 4224-4240, 2021.
- Kim, M., Kim, S. H., Kim, W. V., Lee, Y. G., Kim, J., and Kafatos, M. C.: Assessment of Aerosol optical depth under  
background and polluted conditions using AERONET and VIIRS datasets, *Atmospheric Environment*, 245, 117994, 2021.
- Kim, J., Jeong, U., Ahn, M.-H., Kim, J. H., Park, R. J., Lee, H., Song, C. H., Choi, Y.-S., Lee, K.-H., and Yoo, J.-M., et al.:  
465 New era of air quality monitoring from space: Geostationary Environment Monitoring Spectrometer (GEMS), *Bulletin of the  
American Meteorological Society*, 101, E1-E22, 2020.
- Kim, M., Kim, J., Torres, O., Ahn, C., Kim, W., Jeong, U., Go, S., Liu, X., Moon, K. J., and Kim, D.-R.: Optimal  
estimation-based algorithm to retrieve aerosol optical properties for GEMS measurements over Asia, *Remote Sensing*, 10,  
162, 2018.
- 470 Kleipool, Q., Dobber, M., de Haan, J., and Levelt, P.: Earth surface reflectance climatology from 3 years of OMI data,  
*Journal of Geophysical Research: Atmospheres*, 113, 2008.



- Kwon, H.-A., Park, R. J., Jeong, J. I., Lee, S., González Abad, G., Kurosu, T. P., Palmer, P. I., and Chance, K.: Sensitivity of formaldehyde (HCHO) column measurements from a geostationary satellite to temporal variation of the air mass factor in East Asia, *Atmospheric Chemistry and Physics*, 17, 4673-4686, 2017.
- 475 Lee, Y., Ahn, M.-H., and Kang, M.: The new potential of deep convective clouds as a calibration target for a geostationary UV/VIS hyperspectral spectrometer, *Remote Sensing*, 12, 446, 2020.
- Levelt, P. F., Van Den Oord, G. H., Dobber, M. R., Malkki, A., Visser, H., De Vries, J., Stammes, P., Lundell, J. O., and Saari, H.: The ozone monitoring instrument, *IEEE Transactions on geoscience and remote sensing*, 44, 1093-1101, 2006.
- Loyola, D. G., Gimeno García, S., Lutz, R., Argyrouli, A., Romahn, F., Spurr, R. J., Pedernana, M., Doicu, A., Molina  
480 García, V., and Schüssler, O.: The operational cloud retrieval algorithms from TROPOMI on board Sentinel-5 Precursor, *Atmospheric Measurement Techniques*, 11, 409-427, 2018.
- Miller, S. D., Mills, S. P., Elvidge, C. D., Lindsey, D. T., Lee, T. F., and Hawkins, J. D.: Suomi satellite brings to light a unique frontier of nighttime environmental sensing capabilities, *Proceedings of the National Academy of Sciences*, 109, 15706-15711, 2012.
- 485 Park, S. S., Kim, S.-W., Song, C.-K., Park, J.-U., and Bae, K.-H.: Spatio-temporal variability of aerosol optical depth, total ozone and NO<sub>2</sub> over East Asia: Strategy for the validation to the GEMS Scientific Products, *Remote Sensing*, 12, 2256, 2020.
- Park, J., Choi, W., Lee, H.-M., Park, R. J., Kim, S.-Y., Yu, J.-A., Lee, D.-W., and Lee, H.: Effect of Error in SO<sub>2</sub> Slant Column Density on the Accuracy of SO<sub>2</sub> Transport Flow Rate Estimates Based on GEMS Synthetic Radiances, *Remote Sensing*, 13, 3047, 2021.
- 490 Platt, U., Perner, D., and Pätz, H.: Simultaneous measurement of atmospheric CH<sub>2</sub>O, O<sub>3</sub>, and NO<sub>2</sub> by differential optical absorption, *Journal of Geophysical Research: Oceans*, 84, 6329-6335, 1979.
- Sneep, M., De Haan, J., Stammes, P., Wang, P., Vanbauce, C., Joiner, J., Vasilkov, A., and Levelt, P.: Three-way comparison between OMI and PARASOL cloud pressure products, *Journal of Geophysical Research: Atmospheres*, 113, 2008.
- 495 Spurr, R. J.: VLIDORT: A linearized pseudo-spherical vector discrete ordinate radiative transfer code for forward model and retrieval studies in multilayer multiple scattering media, *Journal of Quantitative Spectroscopy and Radiative Transfer*, 102, 316-342, 2006.
- Stammes, P., Sneep, M., De Haan, J., Veefkind, J., Wang, P., and Levelt, P.: Effective cloud fractions from the Ozone Monitoring Instrument: Theoretical framework and validation, *Journal of Geophysical Research: Atmospheres*, 113, 2008.
- 500 Taylor, T. E., O'Dell, C. W., O'Brien, D. M., Kikuchi, N., Yokota, T., Nakajima, T. Y., Ishida, H., Crisp, D., and Nakajima, T.: Comparison of cloud-screening methods applied to GOSAT near-infrared spectra, *IEEE Transactions on Geoscience and Remote Sensing*, 50, 295-309, 2011.
- Thalman, R. and Volkamer, R.: Temperature dependent absorption cross-sections of O<sub>2</sub>-O<sub>2</sub> collision pairs between 340 and 630 nm and at atmospherically relevant pressure, *Physical chemistry chemical physics*, 15, 15371-15381, 2013.



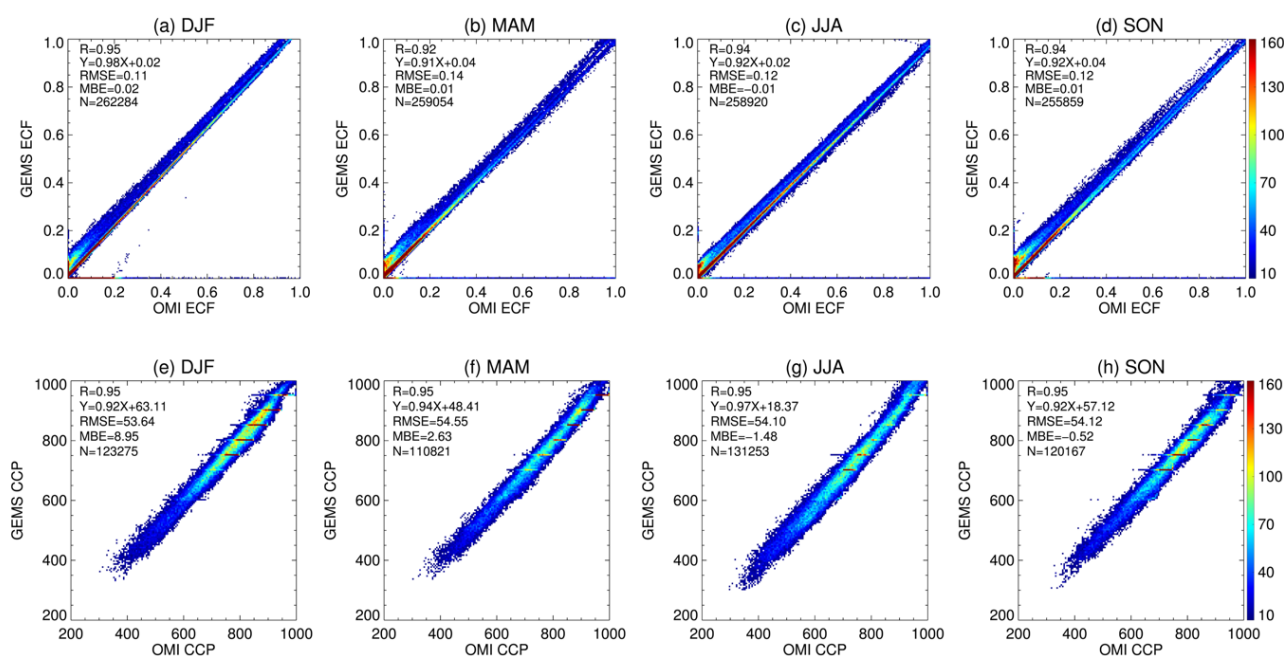
- 505 Vasilkov, A., Joiner, J., Spurr, R., Bhartia, P. K., Levelt, P., and Stephens, G.: Evaluation of the OMI cloud pressures derived from rotational Raman scattering by comparisons with other satellite data and radiative transfer simulations, *Journal of Geophysical Research: Atmospheres*, 113, 2008.
- Vasilkov, A., Yang, E.-S., Marchenko, S., Qin, W., Lamsal, L., Joiner, J., Krotkov, N., Haffner, D., Bhartia, P. K., and Spurr, R.: A cloud algorithm based on the O<sub>2</sub>-O<sub>2</sub> 477 nm absorption band featuring an advanced spectral fitting method and the use  
 510 of surface geometry-dependent Lambertian-equivalent reflectivity, *Atmospheric Measurement Techniques*, 11, 4093-4107, 2018.
- Veefkind, J. P., De Haan, J. F., Sneep, M., and Levelt, P. F.: Improvements to the OMI O<sub>2</sub>-O<sub>2</sub> operational cloud algorithm and comparisons with ground-based radar-lidar observations, *Atmospheric Measurement Techniques*, 9, 6035-6049, 2016.
- Veefkind, J. P., Aben, I., McMullan, K., Förster, H., De Vries, J., Otter, G., Claas, J., Eskes, H., De Haan, J., and Kleipool,  
 515 Q.: TROPOMI on the ESA Sentinel-5 Precursor: A GMES mission for global observations of the atmospheric composition for climate, air quality and ozone layer applications, *Remote sensing of environment*, 120, 70-83, 2012.
- Wang, P. and Stammes, P.: Evaluation of SCIAMACHY Oxygen A band cloud heights using Cloudnet measurements, *Atmospheric Measurement Techniques*, 7, 1331-1350, 2014.
- Wang, P., Stammes, P., Van Der A, R., Pinardi, G., and Van Roozendael, M.: FRESCO+: an improved O<sub>2</sub> A-band cloud  
 520 retrieval algorithm for tropospheric trace gas retrievals, *Atmospheric Chemistry and Physics*, 8, 6565-6576, 2008.
- Wang, S., Liu, C., Zhang, W., Hao, N., Gimeno García, S., Xing, C., Zhang, C., Su, W., and Liu, J.: Development and Application of HECORA Cloud Retrieval Algorithm Based On the O<sub>2</sub>-O<sub>2</sub> 477 nm Absorption Band, *Remote Sensing*, 12, 3039, 2020.
- Winker, D. M., Vaughan, M. A., Omar, A., Hu, Y., Powell, K. A., Liu, Z., Hunt, W. H., and Young, S. A.: Overview of the  
 525 CALIPSO mission and CALIOP data processing algorithms, *Journal of Atmospheric and Oceanic Technology*, 26, 2310-2323, 2009.
- Yang, J., Li, S., Gong, W., Min, Q., Mao, F., and Pan, Z.: A fast cloud geometrical thickness retrieval algorithm for single-layer marine liquid clouds using OCO-2 oxygen A-band measurements, *Remote Sensing of Environment*, 256, 112305, 2021.
- Yoshida, Y., Ota, Y., Eguchi, N., Kikuchi, N., Nobuta, K., Tran, H., Morino, I., and Yokota, T.: Retrieval algorithm for CO<sub>2</sub>  
 530 and CH<sub>4</sub> column abundances from short-wavelength infrared spectral observations by the Greenhouse gases observing satellite, *Atmospheric Measurement Techniques*, 4, 717-734, 2011.

**Table 1:** This is a table for values of each nodal points to calculate the look-up table in GEMS cloud retrieval algorithm.

| Parameters               | Values  |
|--------------------------|---|
| Solar zenith angle (°)   | 0, 18.2, 25.8, 31.8, 36.9, 41.4, 45.6, 49.5, 53.1, 56.6, 60.0, 63.3, 66.4, 69.5, 72.5, 75.5, 78.5, 81.4, 84.3 |
| Viewing zenith angle (°) | 0, 18.2, 25.8, 31.8, 36.9, 41.4, 45.6, 49.5, 53.1, 56.6, 60.0, 63.3, 66.4, 69.5, 72.5, 75.5,                  |



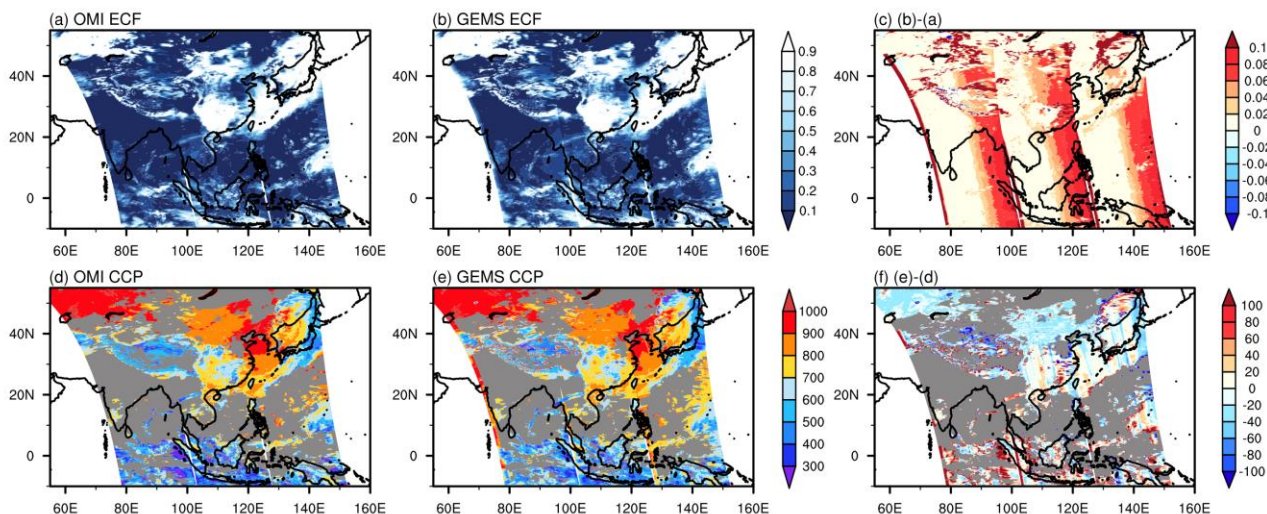
|                               |   |
|-------------------------------|---|
|                               | 78.5, 81.4, 84.3  |
| Relative azimuth angle (°)    | 0, 90, 180  |
| Surface pressure (hPa)        | 1014, 1000, 950, 900, 850, 800, 750, 700, 600, 500, 400, 300, 200, 100  |
| Surface reflectance           | 0, 0.05, 0.1, 0.2, 0.3, 0.4, 0.5, 0.6, 0.7, 0.8, 0.9, 1.0   |
| Effective cloud pressure      | 0, 0.05, 0.1, 0.15, 0.2, 0.25, 0.3, 0.35, 0.4, 0.45, 0.5, 0.55, 0.6, 0.65, 0.7, 0.75, 0.8, 0.85, 0.9, 0.95, 1.0 |
| Cloud centroid pressure (hPa) | 1014, 1000, 950, 900, 850, 800, 750, 700, 600, 500, 400, 300, 200, 100  |



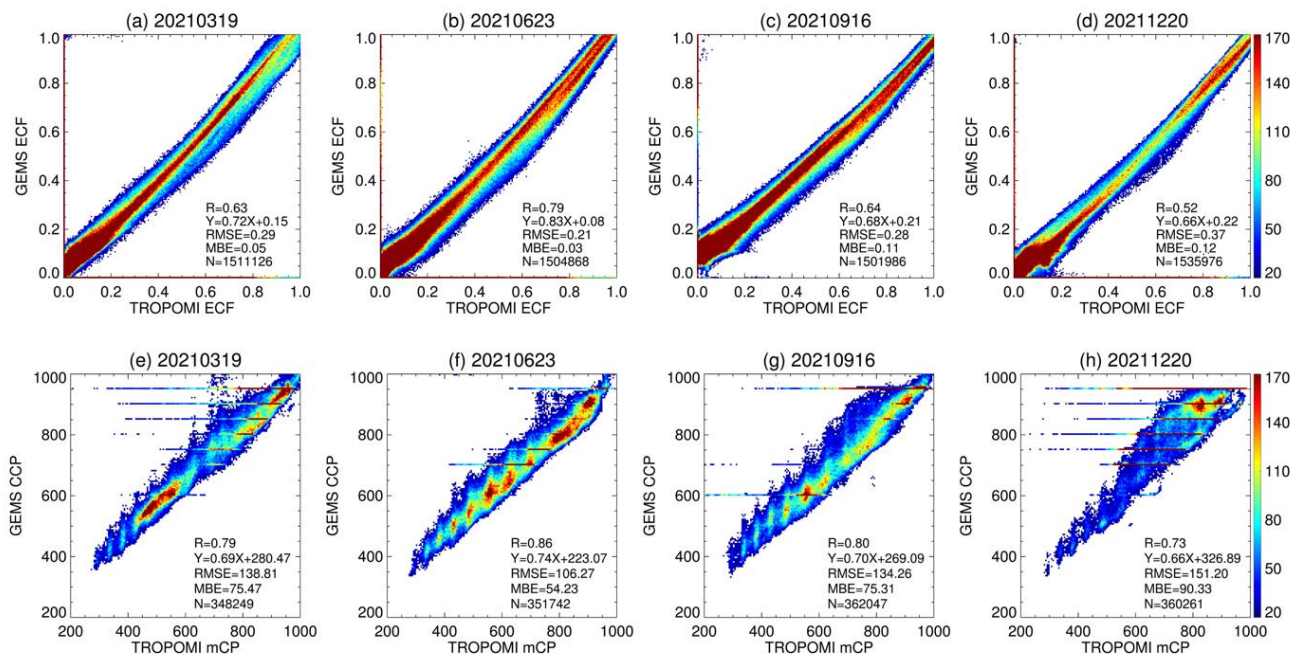
535

**Figure 1: The cloud products for random days in each month of 2007 (classified by seasons: DJF-winter, MAM-spring, JJA-summer, SON-autumn) for comparison with the cloud products from OMI algorithm. The top panel showing the density scatter plot for Effective Cloud Fraction (ECF) and the bottom panel showing the density scatter plot for Cloud Centroid Pressure (CCP). The x-axis represents the values from OMI, and the y-axis represents the cloud products from the GEMS algorithm. The solid line indicates the 1:1 line, and the correlation coefficient (R), regression equation, Root Mean Square Error (RMSE), Mean Bias Error (MBE), and number of pixels (#) used in the analysis are presented.**

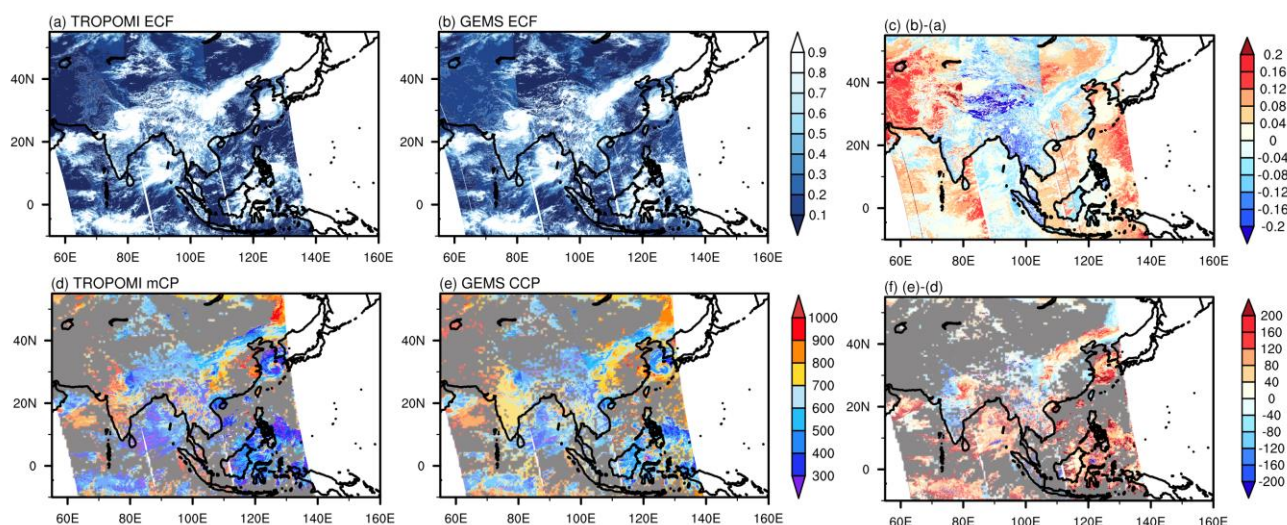
540



545 **Figure 2:** The results using OMI data for performance validation of the GEMS cloud retrieval algorithm. The data from March 5th, 2007 were used as input. (a) shows the ECF provided by OMI, while (b) shows the ECF retrieved by GEMS using OMI L1B data. (d) shows the CCP retrieved by OMI, and (e) shows the CCP image retrieved by GEMS using the OMI radiance data input same as (b). (c) and (f) show the differences in cloud retrieval between the GEMS and OMI algorithms.



550 **Figure 3:** This figure is similar to Figure 1 but for TROPOMI. To verify the performance and seasonal dependency of GEMS cloud algorithm, cloud retrieval results were compared with those of TROPOMI for random days in March, May, September, and December 2021. The top panel shows the results for ECF and the bottom panel shows the results for CCP in a density scatter plot. As the definitions of cloud pressure differ between GEMS and TROPOMI, the density scatter plot was generated using the mean value of CTP and CBP (mean Cloud Pressure, mCP) from TROPOMI. The x-axis shows the TROPOMI values, and the y-axis shows the GEMS cloud retrieval results. The solid line represents the 1:1 line, and the correlation coefficient and regression equation are also displayed.



555

Figure 4: This figure, similar to Figure 2, shows the validation of the GEMS cloud retrieval algorithm using TROPOMI data. Cloud retrievals were performed using observations from September 16, 2021 as input. (a) shows the TROPOMI CF converted to ECF. (b) shows the ECF derived from GEMS using TROPOMI L1B as input. (d) shows the mCP calculated from TROPOMI CTP and CBP, while (e) shows the CCP image retrieved by GEMS cloud retrieval algorithm. (c) and (f) show the differences in cloud retrievals between GEMS and TROPOMI algorithms.

560

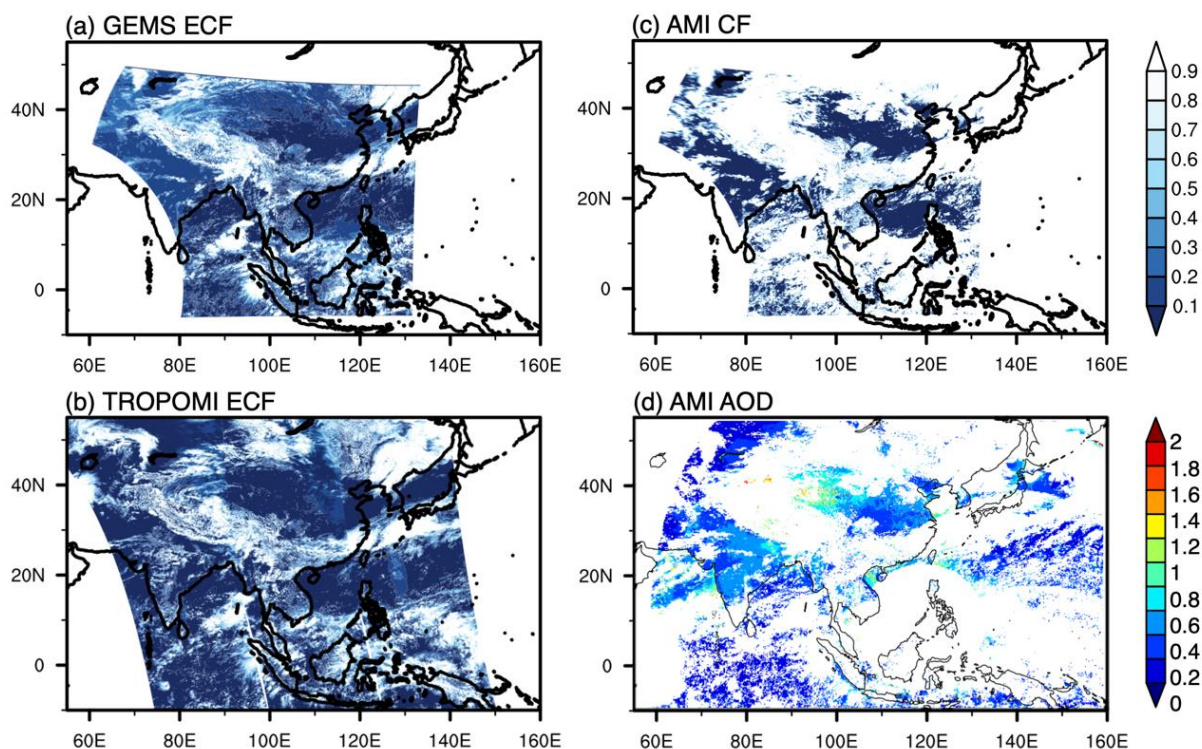
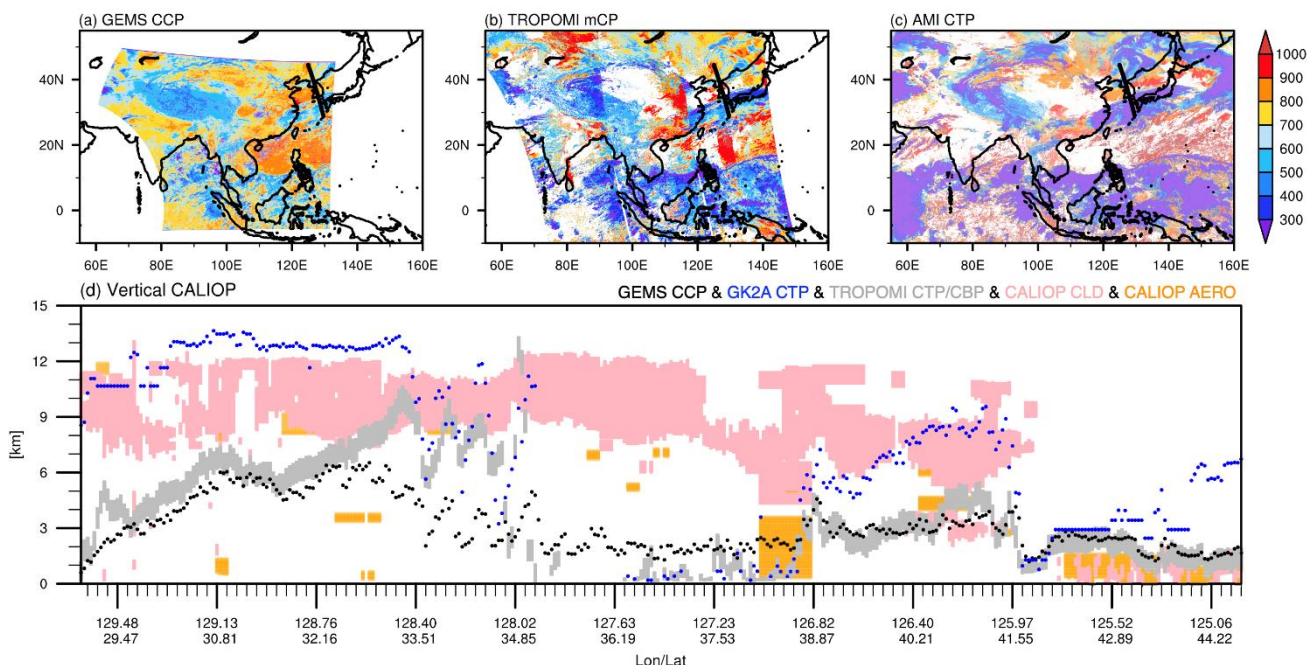


Figure 5: The four different images of air pollutants case observed on May 8, 2021 for GEMS field of view. The first (a) shows the ECF retrieved by GEMS. The second (b) shows the ECF calculated by converting the CF data from TROPOMI. The (c) displays



565

the CF image calculated by collocating AMI data to GEMS pixels. The (d) shows the Aerosol Optical Depth (AOD) image obtained from AMI data.



570

Figure 6: The cloud pressure observation observed on May 8th, 2021. The figure consists of four images (a) GEMS CCP, (b) TROPOMI mCP, (c) AMI CTP, and (d) CALIOP VFM with cloud pressure products. In (a) - (c), the thick black line represents the scan path of CALIOP. In (d), a black dot represents GEMS CCP, a blue dot represents GK2A CTP, the gray shade represents between the TROPOMI CTP and CBP, the pink shade represents CALIOP cloud mask, and the orange shade represents CALIOP aerosol mask.

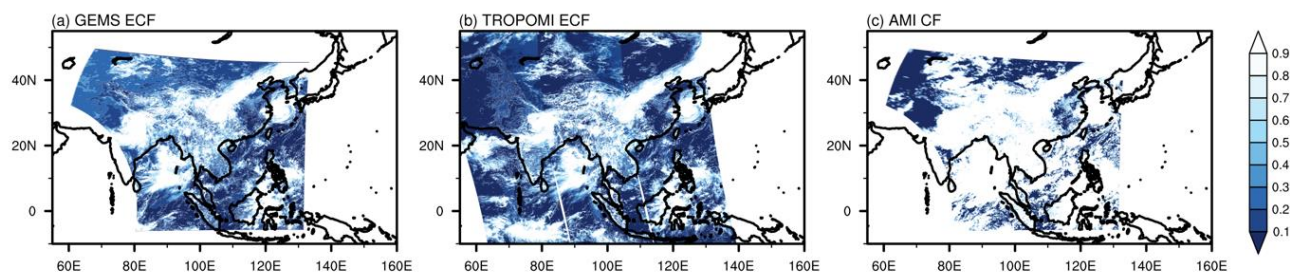
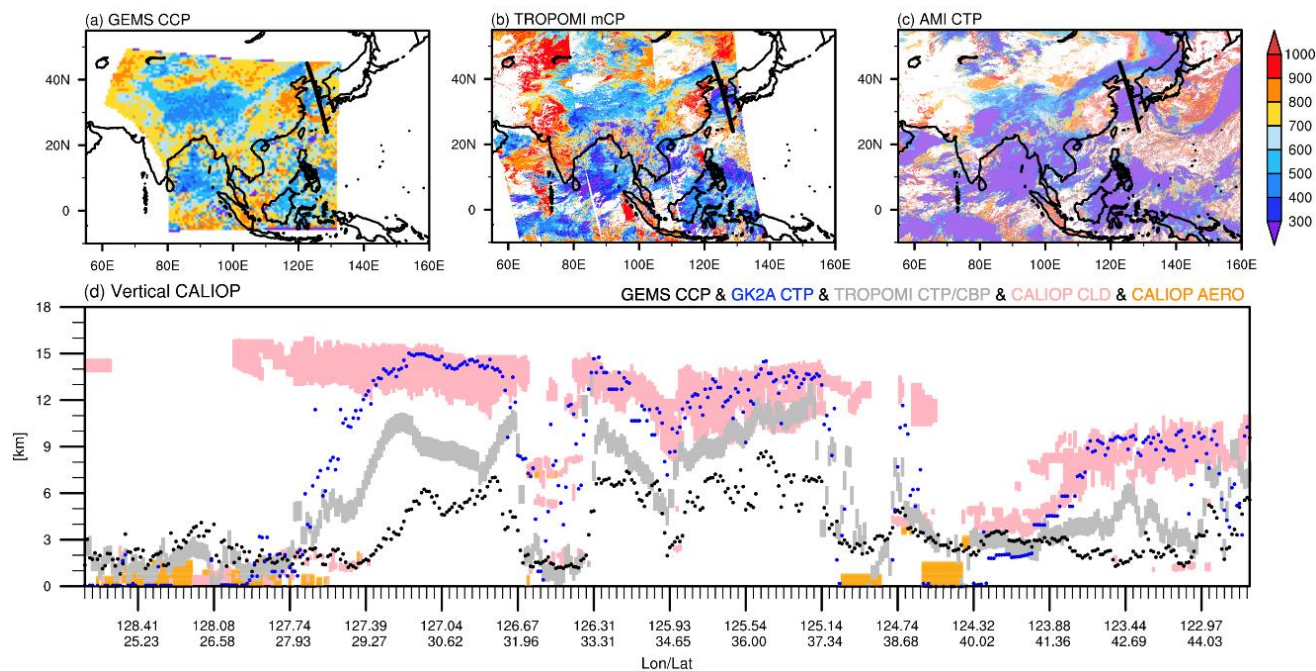
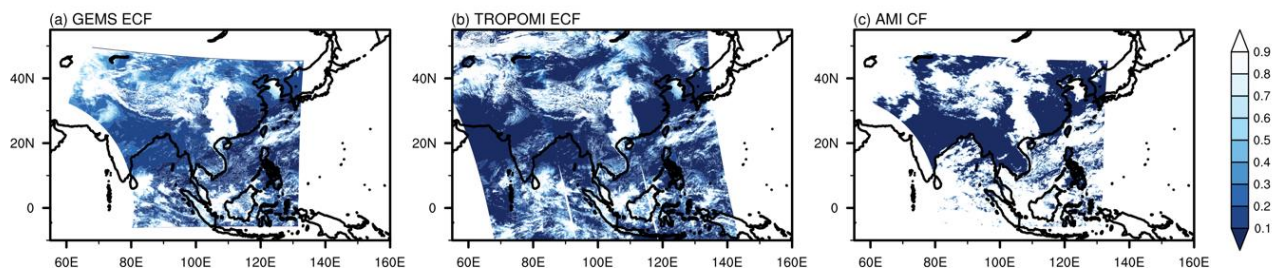


Figure 7: Similar to Figure 5, intercomparison of ECF is presented for the case of Typhoon Chantou, which occurred on September 16, 2021, (a) GEMS ECF, (b) TROPOMI ECF, and (c) AMI CF.



575

**Figure 8:** The case of Typhoon Chantu on September 16, 2021. (a) is the CCP obtained from GEMS, (b) the mCP from TROPOMI, and (c) shows the CTP derived from AMI. (d) overlays the CHs which has been converted to cloud altitude from three satellites onto the CALIOP VFM image.



**580 Figure 9:** Similar to Figure 7, intercomparison of ECF is presented for the case of sea fog, which occurred on March 25, 2021, (a) GEMS ECF, (b) TROPOMI ECF, and (c) AMI CF.

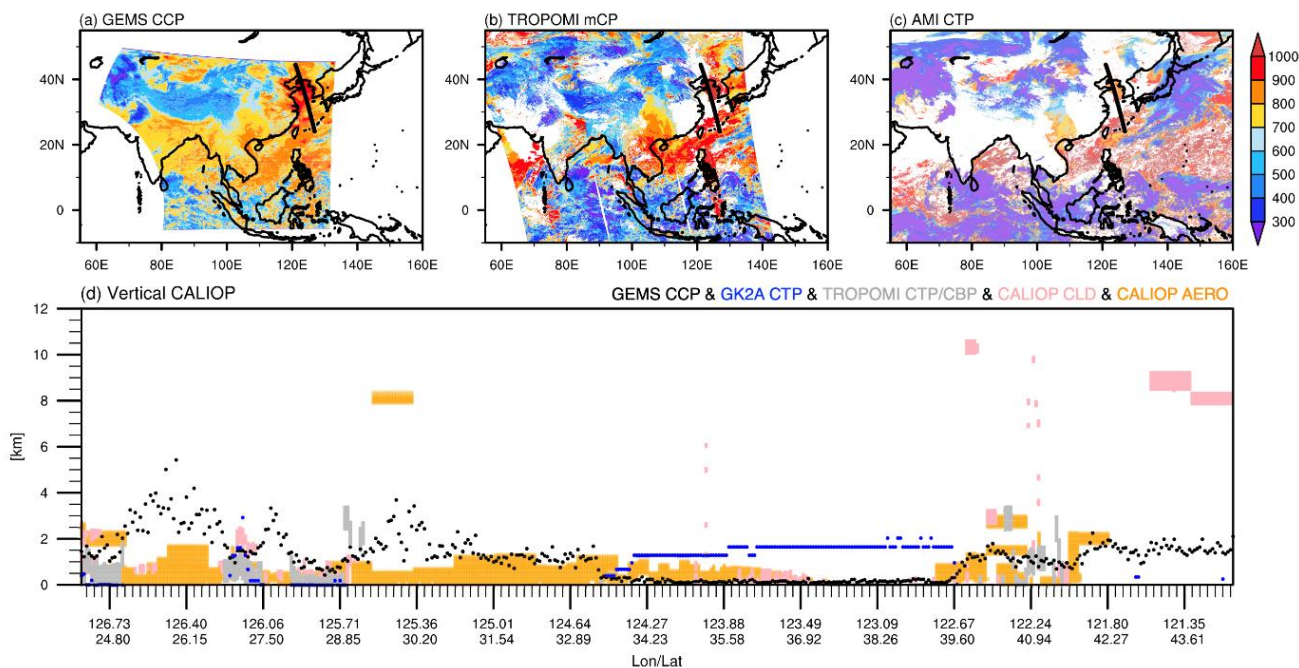


Figure 10: The case of sea fog on March 25, 2021. (a) is the CCP obtained from GEMS, (b) the mCP from TROPOMI, and (c) shows the CTP derived from AMI. (d) overlays the CHs which has been converted to cloud altitude from three satellites onto the CALIOP VFM image.

585